Solution Synthesis of Nanocrystalline M−Zn (M = Pd, Au, Cu) Intermetallic Compounds via Chemical Conversion of Metal Nanoparticle Precursors

Robert E. Cable and Raymond E. Schaak*

Department of Chemistry, Texas A&M University, College Station, Texas 77842-3012

Received May 5, 2007. Revised Manuscript Received May 26, 2007

Alloys and intermetallic compounds offer a wide range of desirable physical and chemical properties. However, accessing these compounds as nanocrystals is not always straightforward, and the continued development of appropriate synthetic pathways is required. Developing processes that are general toward many systems can be particularly challenging, especially when trying to incorporate highly electropositive metals or metals whose precursors are difficult to reduce into alloy or intermetallic compounds using solution chemistry strategies. Here we report a generalized strategy to access nanocrystalline M−Zn intermetallics (M = Au, Cu, Pd) via the chemical conversion of metal nanoparticles using zerovalent organometallic zinc precursors. Using commercially available reagents, transition-metal nanocrystals are made in hot organoamine solvents, which can be further reacted with diethylzinc or diphenylzinc to form intermetallic AuZn, Au_3Zn, Cu_5Zn_8, and PdZn. The reaction pathway from the single-metal precursor to the intermetallic product is confirmed, and the overall particle morphology of the metal nanoparticle precursors is generally conserved in the intermetallic nanoparticle products throughout the conversion reaction. This method offers a general and robust route to zinc-based intermetallics with known catalytic, shape-memory, and corrosion-resistant properties.

Introduction

Alloys of zinc and the late transition metals comprise a diverse class of materials with a range of important structural, catalytic, and electronic properties. Most notably, zinc alloys are desirable materials for their mechanical hardness and corrosion resistance[1] and accordingly are widely used in industry for die casting and coatings. M−Zn intermetallic compounds are also important materials because of their advanced chemical and physical properties, such as catalytic production of H_2[2] and methanol,[3] magnetism,[4] shape-memory effects,[5−7] and tunable surface plasmon resonance (SPR) in colloids.[8] Intermetallic PdZn has shown promise as a catalyst for the steam reformation of methanol for the selective production of H_2 and CO_2, and PdZn is also suspected to be responsible for the high activity and selectivity of ZnO-supported Pd for the same reaction.[2] Similarly, a Cu−Zn alloy formed at the interface of ZnO-supported Cu is suspected to be an active phase for the synthesis of methanol from CO_2 and H_2.[3] Cu−Zn colloids have also been investigated for their optical properties, showing that the SPR band can be tuned over a 60 nm range by varying the alloy composition.[8]

Several strategies have been developed for preparing nanoscale zinc/transition metal alloys and intermetallic compounds. Top-down approaches such as ball-milling have successfully generated binary Zn intermetallics but require reaction times of 20 h or more.[9] Other approaches such as annealing a ZnO-supported transition metal in a reducing atmosphere,[10] electroplating,[11] and laser ablation of bulk M−Zn intermetallics[12] have yielded nanocrystalline materials, but phase-pure products are difficult to achieve, and particle size and morphology are essentially uncontrollable. Solution chemistry routes, which are widely employed for the morphology-controlled synthesis of metal and multimetal nanostructures, have also been used to access nanocrystalline M−Zn compounds. For example, β-CuZn has been synthesized from Cu(II) and Zn(II) salts.[13] However, a harsh and powerful reducing agent is required to reduce the zinc precursor. PdZn has been formed in a two-step reaction from

(1) Budinski, K. G. *Engineering Materials: Properties and Selection*, 4th ed.; Prentice Hall: Englewood Cliffs, NJ, 1992; pp 603−608.
(2) (a) Iwasa, N.; Masuda, S.; Ogawa, N.; Takezawa, N. *Appl. Catal. A* **1995**, *125*, 145−157. (b) Iwasa, N.; Mayanagi, T.; Masuda, S.; Takezawa, N. *React. Kinet. Catal. Lett.* **2000**, *69*, 355−360. (c) Karim, A.; Conant, T.; Datye, A. *J. Catal.* **2006**, *243*, 420−427.
(3) Fujitani, T.; Nakamura, J. *Appl. Catal. A* **2000**, *191*, 111−129.
(4) Liu, L.; Tian, H.; Xie, S.; Zhou, W.; Mu, S.; Song, L.; Liu, D.; Luo, S.; Zhang, Z.; Xiang, Y.; Zhao, X.; Ma, W.; Shen, J.; Li, J.; Wang, C.; Wang, G. *J. Phys. Chem. B* **2006**, *110*, 20158−20165.
(5) Beck, A.; Jan, J. P.; Pearson, W. B.; Templeton, I. M. *Philos. Mag.* **1963**, *8*, 351.
(6) Pops, H.; Massalski, T. B. *T. Metall. Soc. AIME* **1965**, *233*, 728.
(7) Hisatsune, K.; Takuma, Y.; Tanaka, Y.; Udoh, K.; Morimura, T.; Hasaka, M. *Solid State Commun.* **1998**, *106*, 509−512.
(8) Hambrock, J.; Schröter, M. K.; Birkner, A.; Wöll, C.; Fischer, R. A. *Chem. Mater.* **2003**, *15*, 4217−4222.
(9) (a) Ding, C.; Jihua, C.; Hongge, Y.; Zhenhua, C. *Mater. Sci. Eng. A* **2007**, *444*, 1−5. (b) Andrade-Gamboa, J.; Gennari, F. C.; Arneodo Larochette, P.; Neyertz, C.; Ahlers, M.; Pelegrina, J. L. *Mater. Sci. Eng. A* **2007**, *447*, 324−331.
(10) Penner, S.; Jenewein, B.; Gabasch, H.; Klötzer, B.; Wang, D.; Knop-Gericke, A.; Schlögl, R.; Hayek, K. *J. Catal.* **2006**, *241*, 14−19.
(11) Jušėkėnas, R.; Pakštas, V.; Sudavičius, A.; Kapočius, V.; Karpavičienė, V. *Appl. Surf. Sci.* **2004**, *229*, 402−408.
(12) Pithawalla, Y. B.; El-Shall, M. S.; Deevi, S. *Scripta Mater.* **2003**, *48*, 671−676.
(13) Suzuki, N.; Ito, S. *J. Phys. Chem. B* **2006**, *110*, 2048−2086.

10.1021/cm071214j CCC: $37.00
Published on Web 07/07/2007

the thermal decomposition of a heterobimetallic carboxylate-bridged Pd−Zn species followed by reduction under H_2 in a furnace.[14] However, this requires the synthesis of a complex molecular precursor and provides little control over particle size and morphology. Polycrystalline Ni−Zn nanowires have also been synthesized using electrochemical deposition into porous anodic alumina templates.[4]

While these methods have yielded nanoscale M−Zn solids, it remains challenging to rigorously control their morphology (in comparison to capabilities for many single-metal systems), and the synthetic development has largely been limited to the Cu−Zn system. Through the thermolysis of a specially prepared Cu(II) reagent with Et_2Zn, alloy and intermetallic nanocrystals of various Cu−Zn compositions were prepared with some degree of morphological control.[8] Unfortunately, it can be challenging to apply similar chemistry to other M−Zn systems without the need for significant new synthetic development. This issue is part of a broader problem in nanocrystal synthesis—the ability to routinely incorporate electropositive metals or metals whose precursors are not easy to reduce into nanocrystals with the ability to simultaneously control their morphology. Some examples of nanocrystalline alloys and intermetallic compounds containing Al and Mg are accessible using solution chemistry techniques.[15,16] However, very few other examples have been reported, and none have shown evidence of extensive generality or significant morphological control. Generalized strategies for incorporating hard-to-reduce metals into intermetallic nanocrystals using robust solution chemistry techniques could impact several areas of modern materials research that rely on these elements for their properties, including catalysis, structural materials, superconductivity, hydrogen storage, and magnetic materials.

Building on recent synthetic achievements and mechanistic investigations involving nanocrystalline intermetallic compounds of the late transition metals,[17−19] we have been developing "conversion chemistry" approaches for synthesizing morphologically controlled intermetallic nanocrystals.[18−21] This strategy is based on the idea that preformed metal nanoparticles can serve as reactive precursors that can transform into derivative phases using low-temperature chemical reactions. Key examples include the formation of Ag_2Se by reaction of Se with solutions of $AgNO_3$,[22] the synthesis of metal phosphides by reacting metal nanoparticles with trioctylphosphine,[20,23] the shape-controlled formation of M−Sn intermetallics (M = Fe, Co, Ni, Pd) by reaction of β-Sn nanocrystals with appropriate metal precursors,[21] and the stepwise phase interconversion of intermetallic nanocrystals by reaction with metal salt solutions under reducing conditions.[19] These processes generally involve a diffusion-based mechanism, where a zerovalent metal precursor diffuses into the pre-existing metal nanoparticle. In many cases, the shape of the metal nanoparticle precursors can be retained in the final product, providing a potentially generalizable strategy for controlling the morphology of nanocrystals with two or more elements in a compositionally controllable manner. This approach, therefore, capitalizes on advances in the synthesis of single-metal nanoparticles and utilizes them as compositional, morphological, and sometimes structural precursors for the formation of more complex nanocrystals than are often achievable using direct methods.

In this paper, we describe the application of this "conversion chemistry" approach to the formation of Zn-based intermetallic nanocrystals using chemistry that facilitates compositional, structural, and morphological control. Specifically, Zn-based intermetallics are synthesized in a one-pot reaction by adding diethyl zinc (Et_2Zn) or diphenyl zinc (Ph_2Zn) to preformed metal nanocrystals generated in situ. We also show that the chemistry that is developed for one system is portable to several others, providing evidence of generality. Finally, all of the reagents and precursors are commercially available, which is convenient but also important for generalizing the method to other systems in the future. The targets we chose cover a range of useful Zn-based intermetallic nanomaterials. Au−Zn intermetallics can have advanced structural properties, and we have prepared two different phases within this system, β'-AuZn and $Au_3Zn[R_1]$. β'-AuZn is a known shape-memory material,[5,6] and there is evidence that $Au_3Zn[R_1]$ may also undergo reversible martensite transformation.[7] Cu−Zn alloys and intermetallics also have useful structural and corrosion resistant properties.[1] More recently, ZnO-supported Pd catalysts were found to be highly active for the selective production of H_2 and CO_2 via steam reformation of methanol,[2] while ZnO-supported Cu catalysts are active for the production of methanol from CO_2 and H_2.[3] In each case, a Cu− or Pd−Zn intermetallic or alloy is suspected to be responsible for the high activity and selectivity. Here we report the synthesis of nanocrystalline

(14) Tkachenko, O. P.; Stakheev, A. Y.; Kustov, L. M.; Mashkovsky, I. V.; van den Berg, M.; Grünert, W.; Kozitsyna, N. Y.; Dobrokhotova, Z. V.; Zhilov, V. I.; Nefedov, S. E.; Vargaftik, M. N.; Moiseev, I. I. *Catal. Lett.* **2006**, *112*, 155−161.

(15) (a) Bogdanović, B.; Claus, K.-H.; Gürtzen, S.; Spliethoff, B.; Wilczok, U. *J. Less-Common Met.* **1987**, *131*, 163−172. (b) Abe, O.; Tsuge, A. *J. Mater. Res.* **1991**, *6*, 928−934. (b) Jones, D. J.; Rozière, J.; Aleandri, L. E.; Bogdanović, B.; Huckett, S. C. *Chem. Mater.* **1992**, *4*, 620−625. (c) Schwab, S. T.; Paul, P. P.; Pan, Y.-M. *Mater. Sci. Eng.* **1995**, *A202*, 197−200. (d) Lu, Q.; Hu, J.; Tang, K.; Qian, Y.; Zhou, G.; Liu, X. *Solid State Ionics* **1999**, *124*, 317−321. (e) Haber, J. A.; Gunda, N. V.; Balbach, J. J.; Conradi, M. S.; Buhro, W. E. *Chem. Mater.* **2000**, *12*, 973−982. (f) Damle, C.; Gopal, A.; Sastry, M. *Nano. Lett.* **2002**, *2*, 365−368. (g) Bönnemann, H.; Brijoux, W.; Hofstadt, H. -W.; Ould-Ely, T.; Schmidt, W.; Waβmuth, B.; Weidenthaler, C. *Angew. Chem., Int. Ed.* **2002**, *41*, 599−603. (h) Pithawalla, Y. B.; Deevi, S. *Mater. Res. Bull.* **2004**, *39*, 2303−2316. (i) Ma, J.; Du, Y. *J. Alloy Compd.* **2005**, *395*, 277−279.

(16) Cokoja, M.; Parala, H.; Schröter, M.-K.; Birkner, A.; van den Berg, M. W. E.; Grünert, W.; Fischer, R. A. *Chem. Mater.* **2006**, *18*, 1634−1642.

(17) (a) Sra, A. K.; Schaak, R. E. *J. Am. Chem. Soc.* **2004**, *126*, 6667−6672. (b) Sra, A. K.; Ewers, T. D.; Schaak, R. E. *Chem. Mater.* **2005**, *17*, 758−766. (c) Schaak, R. E.; Sra, A. K.; Leonard, B. M.; Cable, R. E.; Bauer, J. C.; Han, Y.-F.; Means, J.; Teizer, W.; Vasquez, Y.; Funck, E. S. *J. Am. Chem. Soc.* **2005**, *127*, 3506−3515. (d) Leonard, B. M.; Bhuvanesh, N. S. P.; Schaak, R. E. *J. Am. Chem. Soc.* **2005**, *127*, 7326−7327. (e) Cable, R. E.; Schaak, R. E. *Chem. Mater.* **2005**, *17*, 6835−6841.

(18) Leonard, B. M.; Schaak, R. E. *J. Am. Chem. Soc.* **2006**, *128*, 11475−11482.

(19) Cable, R. E.; Schaak, R. E. *J. Am. Chem. Soc.* **2006**, *128*, 9588−9589.

(20) Henkes, A. E.; Vasquez, Y.; Schaak, R. E. *J. Am. Chem. Soc.* **2007**, *129*, 1896−1897.

(21) Chou, N. H.; Schaak, R. E. *J. Am. Chem. Soc.* **2007**, *129*, 7339−7345.

(22) Gates, B.; Wu, Y. Y.; Yin, Y. D.; Yang, P. D.; Xia, Y. N. *J. Am. Chem. Soc.* **2001**, *123*, 11500−11501.

(23) Chiang, R.-K.; Chiang, R.-T. *Inorg. Chem.* **2007**, *46*, 369−371.

β_1-PdZn, γ-CuZn (Cu_5Zn_8), β'-AuZn, and $Au_3Zn[R_1]$ using a unified chemical conversion strategy that utilizes preformed Pd, Cu, and Au nanocrystals as precursors.

Experimental Section

Materials. All chemicals were used as received and stored in a glovebox under Ar. The following solvents were used: $CH_3(CH_2)_{15}NH_2$ (1-hexadecylamine, tech 90%, remainder mainly 1-octadecylamine), $CH_3(CH_2)_{17}NH_2$ (1-octadecylamine, 98%), and $CH_3(CH_2)_7NH_2$ (1-octylamine, 99%). The following metal reagents were used: $AuCl_3$ (99.99%), $Au(OOCCH_3)_2$ (99.9%), $Cu(OOCCH_3)_2$ (anhydrous, 98%), $Pd_2(C_{17}H_{14}O)_3$ (Pd content 23.34%), $Zn(C_2H_5)_2$ (diethylzinc, nominally 15% w/w in hexane), and $(C_6H_5)_2Zn$ (diphenylzinc, 98+%). All chemicals were purchased from Alfa Aesar.

Synthesis. The synthetic method relies upon the thermal decomposition or reduction of zerovalent organometallic or metal−salt reagents in a hot organoamine solvent. In short, HDA or a mixture of HDA and ODA were heated in a 100 mL three-neck round-bottom flask under flowing Ar and magnetic stirring. The flask was outfitted with a condenser and thermometer adaptor with a gas inlet. A 1-octylamine solution of the transition metal precursor was injected into the hot organoamine solvent and allowed to age for various amounts of time before a small aliquot was removed in order to probe the reaction pathway. A 1-octylamine solution of Et_2Zn or diphenylzinc (Ph_2Zn) was then added to the reaction, and the temperature was increased if necessary and held at roughly 250 °C for 1 h. After the hour, the reaction was cooled to roughly 30 °C. All aliquots and final products were isolated by centrifugation after the addition of a 3:1 solution of toluene:ethanol and then washed several times with a 1:4 toluene:ethanol solution. After centrifugation, the supernatant solutions generally were completely colorless. This indicates nearly complete reaction of the Au, Cu, and Pd precursors, which were the limiting reagents.

PdZn. $Pd_2(C_{17}H_{14}O)_3$ (2 mL, 12.3 mM in 1-octylamine) was added to 5.1 g of HDA at 250 °C. After 25 min a small aliquot was taken followed by the quick addition of 1 mL of Et_2Zn (0.465 M in 1-octylamine). The solution was held at 250 °C for 1 h.

Cu_5Zn_8. $Cu(OOCCH_3)_2$ (2 mL, 25.1 mM in 1-octylamine) was quickly added to 5.1 g of HDA at 140 °C. After heating to 220 °C, the solution turns from light blue to yellow and then a rusty red/blue, indicating the formation of Cu^0 particles. After taking a small aliquot, 1 mL of Et_2Zn (0.412 M in 1-octylamine) was quickly added and the reaction was heated to 245−250 °C and held for 1 h.

AuZn. $Au(OOCCH_3)_2$ (2 mL, 24.7 mM in 1-octylamine) was quickly added to 5.4 g of HDA at 250 °C. The solution quickly turned pink then deep wine-red, indicating the formation of Au^0 particles. After 10 min, the solution was cooled to 230 °C and 1 mL of Et_2Zn (0.619 M in 1-octylamine) was quickly added. The solution was heated back to 250 °C and held for 1 h and turned a dark black/purple color.

Au_3Zn. $AuCl_3$ (2 mL, 26.5 mM in 1-octylamine) was quickly added to 3.8 g of HDA and 1.0 g of ODA at 120 °C. The solution was slowly heated to 140 °C, and the color changed from yellow to pink then deep wine-red, indicating the formation of Au^0 particles. After taking an aliquot, 1 mL of Ph_2Zn (0.206 M in 1-octylamine) was quickly added. The solution was heated to 225−230 °C and held for 1 h and turned a dark red/brown color.

Characterization. Powder X-ray diffraction (XRD) data were collected on a Bruker GADDS three-circle X-ray diffractometer using Cu Kα radiation. Transmission electron microscopy (TEM) images, selected area electron diffraction (SAED) patterns, and energy-dispersive X-ray analysis (EDS) were collected using a JEOL JEM-2010 TEM. Samples were prepared by sonicating the nanocrystalline metal or intermetallic powders in ethanol or toluene and dropping a small volume onto a carbon-coated copper or nickel grid. Optical spectroscopy was collected by an Agilent 8453 UV−visible spectrophotometer using quartz cuvettes.

Results and Discussion

Long-chain organoamine solvents and zerovalent organometallic reagents have become widely used in the synthesis of metal nanoparticles and have been useful for controlling particle morphology in some systems.[24−27] However, rigorously controlling morphology in multimetal systems, while not unprecedented, is more challenging than in single-metal systems. When relying on the coreduction and/or decomposition of multiple metal reagents, it can be very difficult to find reaction conditions suitable for controlling the morphology of the final product. By utilizing a two-step process, we find that the morphology of the intermetallic M−Zn product may be templated by the morphology of the single-metal nanoparticle precursors, which is much easier to control. Accordingly, our "conversion chemistry" route to M−Zn intermetallics involves two distinct steps: the formation of transition metal nanocrystals by the thermolysis or reduction of commercially available reagents and their subsequent transformation into M−Zn intermetallics upon reaction with organozinc reagents (e.g., Et_2Zn) in a hot organoamine solvent. Hot hexadecylamine (HDA) can liberate Zn(0) from Et_2Zn,[8] which can then diffuse into the nanocrystalline metal precursors, eliminating the need for strong reducing agents. (Et_2Zn is highly reactive and ZnO impurities are sometimes seen by us and others[8] even when using rigorously air-free conditions. However, these can be minimized or eliminated by employing careful synthetic techniques and possibly postsynthesis workup.) The organoamine solvent likely doubles as a surface stabilizing agent, which is consistent with the high particle solubility observed in nonpolar solvents like toluene and aggregation and precipitation in polar solvents such as ethanol.

The Pd−Zn system provides a representative example of the two-step synthetic pathway used to generate nanocrystalline M−Zn intermetallics. Pd nanoparticles were first synthesized by injecting a 1-octylamine solution of tris(dibenzylideneacetone)dipalladium(0) into HDA at 250 °C. After aging the dispersion for 30 min, a solution of Et_2Zn in 1-octylamine was quickly injected. The powder XRD patterns (Figure 1) for the Pd precursor and PdZn product, consistent with the simulated patterns for each phase, confirm that Pd nanocrystals were formed first and then converted to PdZn.

(24) (a) Dinega, D. P.; Bawendi, M. G. *Angew. Chem., Int. Ed.* **1999**, *38*, 1788−1791. (b) Sun, S.; Murray, C. B.; Weller, D.; Folks, L.; Moser, A. *Science* **2000**, *287*, 1989−1992. (c) Puntes, V. F.; Zanchet, D.; Erdonmez, C. K.; Alivisatos, A. P. *J. Am. Chem. Soc.* **2002**, *124*, 12874−12880. (d) Chaudret, B. *C. R. Phys.* **2005**, *6*, 117−131.
(25) (a) Hou, Y.; Gao, S. *J. Mater. Chem.* **2003**, *13*, 1510−1512. (b) Shao, H.; Huang, Y.; Lee, H.-S.; Suh, Y. J.; Kim, C.-O. *J. Appl. Phys.* **2006**, *99*, 08N702. (c) Wu, H. P.; Ge, M. Y.; Yao, C. W.; Wang, Y. W.; Zeng, Y. W.; Wang, L. N.; Zhang, G. Q.; Jiang, J. Z. *Nanotechnology* **2006**, *17*, 5339−5343.
(26) Hambrock, J.; Becker, R.; Birkner, A.; Weiβ, J.; Fischer, R. A. *Chem. Commun.* **2002**, 68−69.
(27) Hiramatsu, H.; Osterloh, F. E. *Chem. Mater.* **2004**, *16*, 2509−2511.

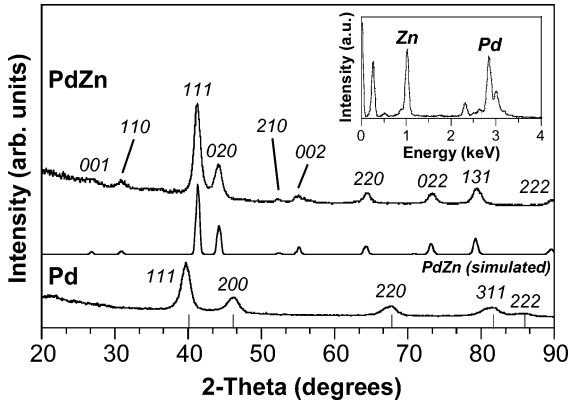

Figure 1. Powder XRD patterns of nanocrystalline Pd precursor and intermetallic PdZn formed after reaction with Et_2Zn. Tick marks correspond to the allowed reflections for Pd, and the simulated XRD pattern for PdZn confirms that the final product is AuCu-type PdZn. EDS (inset) confirms that both Pd and Zn are present in the final product in the expected 1:1 ratio.

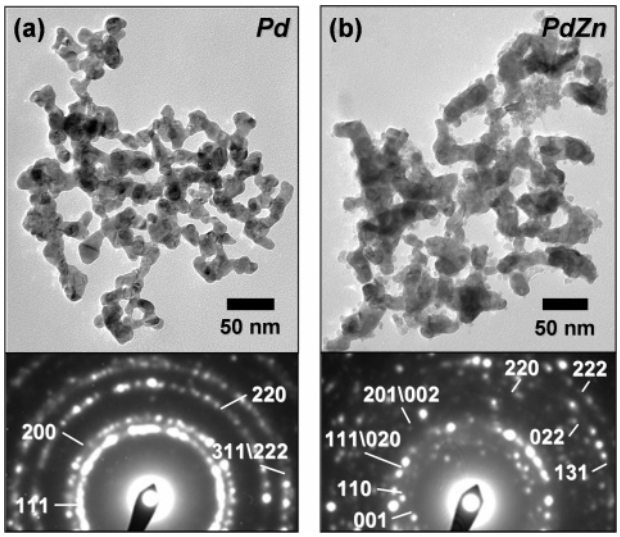

Figure 2. TEM micrographs and corresponding SAED patterns for (a) the nanocrystalline Pd precursor and (b) the intermetallic PdZn product after conversion. SAED patterns match those expected for Pd and PdZn (compare indexing with XRD data in Figure 1).

A TEM micrograph of the Pd nanoparticles isolated from the reaction immediately before the addition of Et_2Zn is shown in Figure 2a, along with the accompanying selected area electron diffraction (SAED) pattern. The data confirm that the reaction pathway begins with the formation of Pd particles, which are then converted to PdZn. The Pd precursor is an interconnected network of nanocrystalline Pd particles with characteristic sizes that range from roughly 5 to 20 nm. The final PdZn product, formed from the reaction of the Pd precursor with Et_2Zn, retains the morphology defined by the precursor (Figure 2b). The interconnected network of PdZn particles grew to an upper-limit diameter of 30 nm. Such particle growth is expected and in fact is required by the addition of Zn to the Pd particles via a diffusion-based mechanism. Data from XRD, TEM, SAED (Figures 1 and 2), and EDS (Figure 1) collectively confirm the morphology-conserving chemical transformation of nanocrystalline Pd (fcc structure) into nanocrystalline β_1-PdZn (AuCu structure).

Intermetallic Cu−Zn nanocrystals can also be generated using similar chemistry. In this case, a solution of copper-

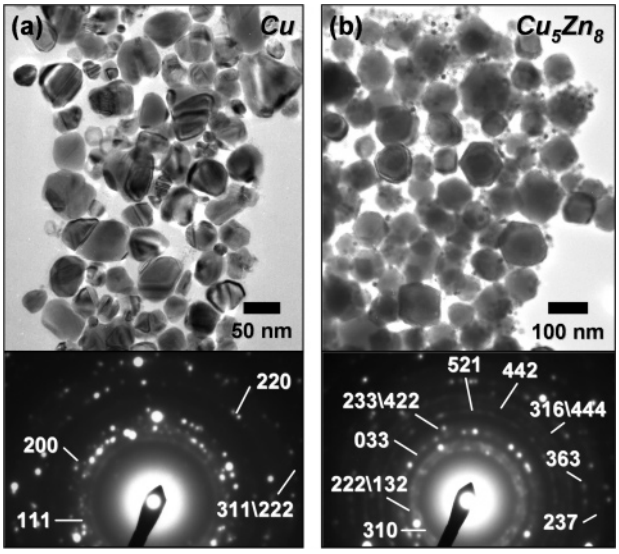

Figure 3. TEM micrographs and corresponding SAED patterns for (a) the nanocrystalline Cu precursor and (b) the intermetallic Cu_5Zn_8 product after conversion. SAED patterns match those expected for Cu and Cu_5Zn_8 (compare indexing with XRD data in Figure 4).

(II) acetate was injected into hot HDA (140 °C) and the temperature was slowly raised to 220 °C. At this temperature, the solution starts to turn a rusty-red color, indicating the reduction of Cu^{2+} to Cu^0 colloids. At high temperatures, organoamines are known to reduce metal salts, their reducing power resulting from the oxidation of the amine groups to nitriles.[27,28] TEM analysis of an aliquot taken from this solution reveals irregularly shaped, multifaceted nanocrystals ranging in size from roughly 20 to 60 nm (Figure 3a), and XRD and SAED confirm that these are Cu nanocrystals as expected. This morphology is similar to a previous report of Cu nanocrystals that were made in hot TOPO,[26] as well as a report of Cu nanocrystals being made in reverse micelles upon reduction by hydrazine.[29] Et_2Zn was added several minutes after the color change, and the solution was heated to 250 °C and held at that temperature for 1 h. The product is γ-Cu_5Zn_8 based on powder XRD (Figure 4) and SAED (Figure 3b), and EDS data confirm the correct composition (Figure 4).

TEM micrographs show that the Cu_5Zn_8 final product often consists of a bidisperse distribution of 10−15 and 70−100 nm particles that are quasispherical and multifaceted. A shell of lighter contrast, which is most likely ZnO, can be seen in all of the products but most easily in the smaller particles (Figure S1). The smaller particles are possibly the result of the low-temperature preparation of the Cu precursor particles discussed above. Because Et_2Zn is added to the reaction mixture a few minutes after the first signs of Cu reduction, the reduction may not be complete under these conditions. When the temperature is increased to 250 °C and existing particle growth is occurring, some of the remaining Cu(II) may be reduced to form very small Cu particles that react

(28) (a) Clarke, T. G.; Hampson, N. A.; Lee, J. B.; Morley, J. R.; Scanlon, B. *Tetrahedron Lett.* **1968**, *54*, 5685−5688. (b) Capdevielle, P.; Lavigne, A.; Sparfel, D.; Baranne-Lafont, J.; Cuong, N. K.; Maumy, M. *Tetrahedron Lett.* **1990**, *31*, 3305−3308.
(29) Salzemann, C.; Lisiecki, I.; Urban, J.; Pileni, M. P. *Langmuir* **2004**, *20*, 11772−11777.

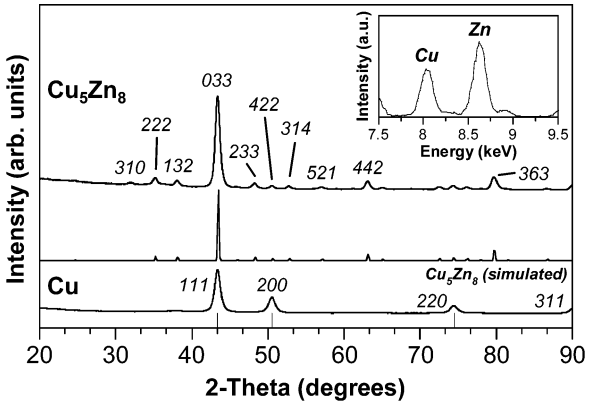

Figure 4. Powder XRD patterns of nanocrystalline Cu precursor and intermetallic Cu_5Zn_8 formed after reaction with Et_2Zn. Tick marks correspond to the allowed reflections for Cu, and the simulated XRD pattern confirms that the final product is Cu_5Zn_8. EDS (inset) confirms that Cu and Zn are present in the final product in a 37:63 ratio, which is close to that expected for Cu_5Zn_8.

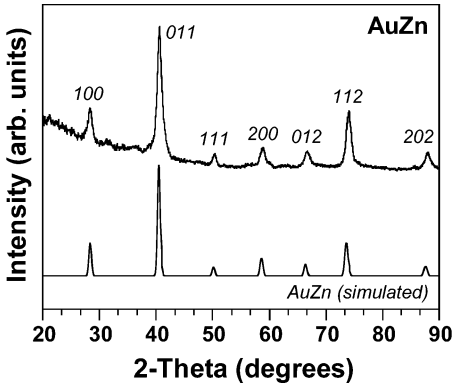

Figure 5. Powder XRD pattern of nanocrystalline intermetallic AuZn. A number of small peaks between 30° and 40° 2θ are due to a slight ZnO impurity in the product.

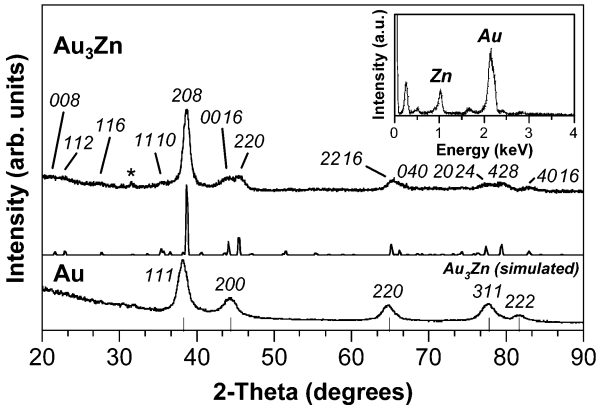

Figure 6. Powder XRD patterns of nanocrystalline Au precursor and intermetallic Au_3Zn formed after reaction with Ph_2Zn. Tick marks correspond to the allowed Au reflections, and the simulated XRD pattern for Au_3Zn confirms that the final product is $Au_3Zn[R_1]$. EDS (inset) confirms that Au and Zn are present in the final Au_3Zn product in a 70:30 ratio, which is within the range of stability for the phase. A small ZnO impurity is labeled with an asterisk (*).

to form Cu_5Zn_8. (There is no XRD, SAED, or EDS evidence for Cu or Zn metal in the final product.) Consistent with this hypothesis, the population of small particles can be minimized by modifying the reaction conditions. For example, injecting the copper(II) acetate at 250 °C followed by the addition of Et_2Zn after 20 min results in quasispherical Cu_5Zn_8 particles that range in size from 50 to 100 nm, as seen in Figure S1 along with the accompanying XRD and SAED patterns (Figure S2). The higher temperature addition of copper(II) acetate likely facilitates a more complete reduction of Cu(II), resulting in a more uniform Cu precursor particle population. This hypothesis is consistent with TEM images of the final product (Figure S1), as well as literature reports for solution routes to Cu and Cu−Zn nanocrystals.[8,30] No attempt was made to rigorously control the morphology or size dispersity of the Cu nanoparticle precursors because Cu_5Zn_8 nanocrystals have been reported previously using other methods.[8,13,30] Rather, our focus was on establishing that the Cu_5Zn_8 phase can be synthesized using the same chemical conversion strategy that works for several other systems. However, literature methods exist for rigorously controlling the synthesis of Cu nanocrystals,[26,29,31] so it may be possible to access Cu_5Zn_8 nanocrystals with different sizes, size dispersities, and shapes using such nanocrystals as morphological templates.

For the Au−Zn system, care was taken to generate high-quality Au nanocrystals as precursors in order to study the ability of this strategy to rigorously retain the morphology and size dispersity of the metal nanoparticle precursor in the M−Zn product. We find that two phases in the Au−Zn system are accessible using this general synthetic method. CsCl-type β'-AuZn can be synthesized by the reaction of Au nanoparticles formed from gold(III) acetate with Et_2Zn in HDA at 250 °C (Figure 5). However, obtaining a phase-pure product was very difficult. In contrast, the long-period ordered phase $Au_3Zn[R_1]$ can be routinely synthesized by using gold(III) chloride as the Au source. We found that that the final product phase depends on the reagent that is used in the synthesis. For example, Au_3Zn is the preferred phase when using $AuCl_3$ as the gold source, while AuZn is preferred when using Au(III) acetate.

A solution of $AuCl_3$ in 1-octylamine was injected into a mixture of HDA and 1-octadecylamine (ODA) at 130 °C. The solution slowly turns pink, then deep wine-red, which indicates the formation of Au nanoparticles. Powder XRD (Figure 6) and SAED (Figure 7a) confirm the formation of Au nanoparticles, and the TEM micrograph in Figure 7a shows that monodisperse 10 ± 1 nm Au particles formed from this reaction. Within a few minutes after the color change, a 1-octylamine solution of diphenyl zinc (Ph_2Zn) was quickly injected, and the reaction was aged at 240 °C for 1 h. Ph_2Zn was chosen as the zinc source for this reaction because it is a powder and more resistant to oxidation than Et_2Zn, and it allowed us to routinely produce phase-pure Au_3Zn without any observable impurities.

Powder XRD confirms the formation of $Au_3Zn[R_1]$ from the reaction of Au nanoparticles with Ph_2Zn. The final Au_3Zn particles retain the overall monodispersity and spherical

(30) Cokoja, M.; Parala, H.; Schröter, M. K.; Birkner, A.; van den Berg, M. W. E.; Klementiev, K. V.; Grünert, W; Fischer, R. A. *J. Mater. Chem.* **2006**, *16*, 2420−2428.

(31) (a) Tanori, J.; Pileni, M. P. *Langmuir* **1997**, *13*, 639−646. (b) Pileni, M. P.; Gulik-Krzywicki, T.; Tanori, J.; Filankembo, A.; Dedieu, J. C. *Langmuir* **1998**, *14*, 7359−7363. (c) Ren, X.; Chem, D.; Tang, F. *J. Phys. Chem. B* **2005**, *109*, 15803−15807. (d) Wang, Y.; Chen, P.; Liu, M. *Nanotechnology* **2006**, *17*, 6000−6006. (e) Zhou, G.; Lu, M.; Yang, Z. *Langmuir* **2006**, *22*, 5900−5903.

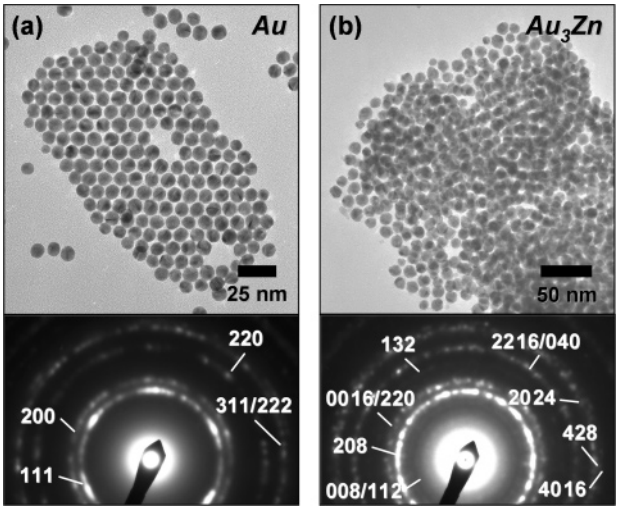

Figure 7. TEM micrographs and corresponding SAED patterns for (a) the Au nanocrystal precursor and (b) the intermetallic Au_3Zn product after reaction with Ph_2Zn. SAED patterns match those expected for Au and Au_3Zn (compare indexing with XRD data in Figure 6).

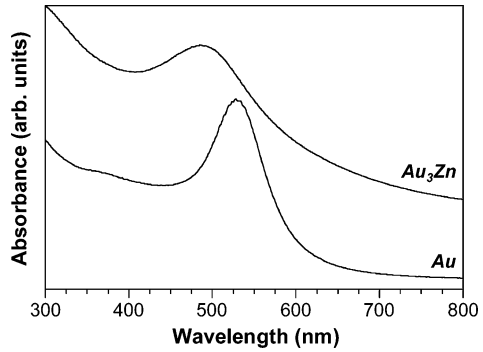

Figure 8. UV−visible absorption spectrum of (bottom) the Au precursor nanocrystals and (top) the Au_3Zn product nanocrystals after conversion. Both precursor and product were suspended in toluene.

morphology of the Au nanoparticle precursors, with the average size increasing to approximately 11 ± 1.5 nm (Figure 7b). The particles become slightly faceted after the conversion, and this result was observed in the Cu−Zn system as well.[8] The SAED pattern for the Au_3Zn product was indexed (Figure 7b) and is consistent with the simulated Au_3Zn[R1] XRD pattern. EDS analysis shows that the composition is consistent with Au_3Zn as well (Figure 6).

Colloidal suspensions of the Au intermediate and Au_3Zn intermetallic product in toluene were analyzed by UV−visible spectroscopy (Figure 8). Au nanoparticles are well-known to have a visible-wavelength SPR band and it is highly likely that alloying with Zn will tune its position, in analogy to Cu−Zn systems that were reported previously.[8,13,30] The Au nanoparticle precursors absorb strongly with λ_{max} at 534 nm, which correlates well with the expected SPR peak position of similar Au nanoparticles in toluene.[27,32] The intermetallic Au_3Zn nanocrystals exhibit a significant blue-shift, with λ_{max} decreasing to 490 nm. This blue shift also occurs for Cu−Zn alloys and intermetallics with respect to pure copper.[8,13,30]

Unlike many of the binary intermetallics we have focused on in the past, the M−Zn phases presented here are not line

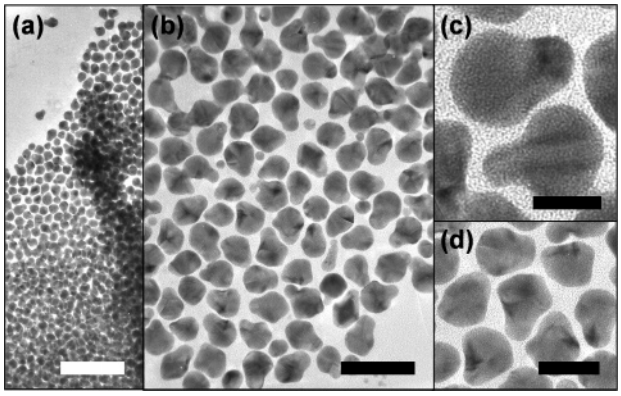

Figure 9. TEM images of anisotropic Au_3Zn nanoparticles with "bicycle seat" morphology formed using higher concentrations of Ph_2Zn (see the text for details). Scale bars are (a) 100 nm, (b) 40 nm, (c) 10 nm, and (d) 20 nm.

phases and as such are stable over a range of compositions. When working with Au_3Zn[R_1], an interesting morphological change is seen when a higher concentration of the Zn reagent is used during synthesis. Starting from spherical Au particles, as seen in Figure 7a, the conversion to Au_3Zn using a higher Zn:Au ratio than used previously seems to induce an anisotropic particle growth, as the final product shows a significant population of particles with a "bicycle seat" morphology (Figure 9). While this tendency toward anisotropic morphology is slightly discernible in the Au_3Zn formed with less Zn reagent, preliminary evidence suggests that a larger concentration of Zn reagent results in more anisotropic particles and a higher degree of anisotropy. However, this typically also results in a larger amount of ZnO impurities in the sample.

Conclusions

In this paper, we have demonstrated a general strategy for the solution-mediated synthesis of nanocrystalline zinc-based intermetallic compounds. Our approach, the result of ongoing investigations of reaction pathways in the synthesis of multimetal nanocrystals,[18−21] involves the low-temperature chemical conversion of preformed metal nanocrystals into intermetallics via reaction with zerovalent organozinc reagents such as Et_2Zn and Ph_2Zn. This strategy appears general, yielding morphologically controllable nanocrystalline intermetallics in the Pd−Zn, Cu−Zn, and Au−Zn systems using commercially available reagents. This work complements some nice chemistry reported by other groups[8,13,30] for the synthesis of nanocrystalline Zn-containing alloys and intermetallics, providing an alternative strategy that is both general and robust. While chemically related to some other strategies for generating M−Zn nanocrystals,[8,13,30] our studies rigorously identify and characterize the crucial role of metal nanoparticles as precursors that have a significant influence on the morphologies of the resulting M−Zn nanocrystals and exploit this to generate a range of morphologies in several systems using standard reagents.

Zinc-based intermetallics are an important addition to the growing library of bimetallic compounds accessible as nanocrystals using straightforward solution routes. The M−Zn intermetallics reported here, as well as other related

(32) Jana, N. R.; Gearheart, L.; Murphy, C. J. *Langmuir* **2001**, *17*, 6782−6786.

compounds, have a range of useful structural, catalytic, and electronic properties, and the ability to access them as nanocrystals using a robust and unified strategy has the potential to expand their applications in these areas. For example, nanocrystalline shape memory alloys such as AuZn could serve as precursors for elaborate nanostructured and microstructured actuators[33] formed via solution-mediated or infiltration-based templating (regardless of their morphology or regularity) followed by low-temperature annealing. Also, nanocrystalline materials can exhibit superplastic behavior,[34] and being able to incorporate additional physical properties such as magnetism or corrosion resistance into such materials may open doors to more advanced applications. The development of facile routes for synthesizing these compounds as nanocrystals is vital to advancing their incorporation into new materials, devices, and processes.

This chemical conversion pathway that results in the formation of M−Zn intermetallic nanocrystals also is important for the realization of additional advances in the synthesis of complex nanocrystalline solids. First, this process represents a quick and easy route to morphologically controllable intermetallics comprised of metals that are difficult to reduce as salts without the use of strong reducing agents. Applying this strategy to additional systems could allow for the incorporation of many other hard-to-reduce metals into intermetallics that are otherwise difficult to synthesize as nanoscale solids using solution chemistry routes. Such capabilities would expand the range of accessible materials for applications in catalysis, superconductivity, magnetism, hydrogen storage, etc. Second, this method has the potential to accommodate rigorous control over particle size and morphology for intermetallic nanoparticles. There are several reports of single-metal nanocrystal systems for which size and shape control is achievable using organoamine solvents like those used here.[25−27] Our results demonstrate that these metal nanoparticles can be used as precursors to M−Zn intermetallics with compelling evidence that morphology is preserved upon conversion to the intermetallic product. This capability is highly relevant for the development of new technologies involving catalysts, shape memory materials, and optically active nanomaterials, as well as fundamental scientific investigations of size−shape−property interrelationships in well-controlled nanomaterials

Acknowledgment. This work was supported by the U.S. Department of Energy (DE-FG02-06ER46333), the Robert A. Welch Foundation (Grant No. A-1583), and the Texas Advanced Research Program (Grant No. 010366-0002-2006). Partial support was also provided by the Arnold and Mabel Beckman Foundation (Young Investigator Award) and DuPont (Young Professor Grant). Electron microscopy was performed at the Texas A&M Microscopy and Imaging Center.

Supporting Information Available: Additional XRD, TEM, EDS, and SAED data. This material is available free of charge via the Internet at http://pubs.acs.org.

CM071214J

(33) (a) Ullakko, K. *J. Mater. Eng. Perform.* **1996**, *5*, 405−409. (b) Huang, W. *Mater. Des.* **2002**, *23*, 11−19. (c) Fu, Y.; Du, H.; Huang, W.; Zhang, S.; Hu, M. *Sensor. Actuat. A-Phys.* **2004**, *112*, 395−408.

(34) McFadden, S. X.; Mishra, R. S.; Valiev, R. Z.; Zhilyaev, A. P.; Mukherjee, A. K. *Nature* **1999**, *398*, 684−686.